International Journal of Automotive and Mechanical Engineering (IJAME)
ISSN: 2229-8649 (Print); ISSN: 2180-1606 (Online); Volume 7, pp. 924-939, January-June 2013

DOI: http://dx.doi.org/10.15282/ijame.7.2012.10.924-939

COMPLIANCE ANALYSIS, OPTIMISATION AND COMPARISON OF A NEW 3PUS-PU MECHANISM

B. Wei

Department of Equipment Manufacturing, Hebei University of Engineering,
056038, Handan, China
E-mail: brave.1987@163.com
Phone: +86-15833094017

ABSTRACT

This paper investigates the compliance of a new 3PUS-PU hybrid mechanism with three degrees of freedom, including translation along the Z axis and rotations about the X and Y axes. Firstly, the kinematic analysis of the mechanism is analysed and the compliance model of the mechanism derived. Secondly, the effects the geometric parameters and position and orientation parameters on the compliance of the mechanism in each direction are investigated, and the genetic algorithm is used to optimise the global compliance by simultaneously adjusting design variables. Finally, the compliance of two similar kinds of 3PUS-PU mechanism in each direction is reviewed.

Keywords: Parallel mechanism; compliance; global compliance optimisation; compliance comparison.

INTRODUCTION

Over the past decade, parallel mechanisms have been widely used in various applications (Patel and George, 2012), such as in machine tools (Hu et al., 2006; Tsai and Joshi, 2002; Xi et al., 2004; Zhang et al., 2005), sensor devices (Zhang et al., 2009), automotive industries (Yu, 2010), medical devices (Li and Xu, 2008; Pan, 2011), mining industries (Wu et al., 2011), etc. This is largely due to the fact that parallel mechanisms possess several advantages compared to their serial counterparts, such as a high stiffness, high precision, high payload capacity, good acceleration, etc. These attributes all contribute to the structure of parallel mechanisms, in which the moving platform is connected to the base by several parallel limbs. Stiffness or compliance is a vital factor in evaluating the performance of parallel manipulators, since a high stiffness can lead to high precision (Zhang, 2009). Here a new 3-DOF hybrid mechanism is proposed, where the moving platform is connected to the base by three active legs and a central passive leg. The compliance matrix of the new mechanism is derived based on the kinetostatic model and principle of virtual work. The effects the geometric parameters and position and orientation parameters on the compliance of the mechanism in each direction are analysed. The leading diagonal element of the compliance matrix is the manipulator's pure compliance in each direction, and the sum of the leading diagonal elements of the compliance matrix is defined as the global compliance. Global compliance is related to system rigidity; subsequently we optimise the global compliance by adjusting the design variables. Finally we compared the new mechanism with a mechanism in which the guide-ways are intersecting each other, and we found that under very small structural parameters the compliance of the mechanism with intersecting guide-ways in each direction are greater than those of the new mechanism with parallel guide-ways, while under larger structural parameters the compliance of the mechanism with intersecting guide-ways in each direction are smaller than those of the new mechanism with parallel guide-ways.

KINEMATIC ANALYSIS OF THE 3PUS-PU MECHANISM

This new 3PUS-PU has three degrees of freedom, which are a translation along the Z axis and rotations around the X and Y axes. There are three identical active legs and one central passive leg. The active leg connects the moving platform by a spherical joint, and the other end connects to the universal joint that is actuated in the guide-way. The guide-ways are parallel to each other. The central passive leg is fixed on the base, and consists of a prismatic joint, another moving link and a universal joint attached to the centre of the moving platform. Fig. 1 provides a schematic representation of the new 3PUS-PU mechanism. For the purpose of analysis, the fixed coordinate frame O_b(X,Y,Z) is attached to the centre of the base, and the moving coordinate frame O_e(x,y,z) is attached to the centre of the moving platform. The radius of the base is R, the radius of the moving platform is r, and l is the length of the active legs.

The position vector of B_i with respect to the fixed frame can be expressed as ${P_{bi}}^b$; the position vector of E_i with respect to the moving frame can be expressed as ${P_{ei}}^e$; the position vector of O_e with respect to the fixed frame can be expressed as P_e^b. α_i is the angle between the X axis and the attachment point B_i on the base, and β_i is the angle between the Z axis and the attachment point E_i on the moving platform. Then one can obtain the following:

$$ {P_{bi}}^b = \begin{bmatrix} R\cdot\cos\alpha_i \\ R\cdot\sin\alpha_i \\ 0 \end{bmatrix}, \quad {P_{ei}}^e = \begin{bmatrix} 0 \\ -r\cdot\sin\beta_i \\ r\cos\beta_i \end{bmatrix}, \quad P_e^b = \begin{bmatrix} 0 \\ 0 \\ z_e \end{bmatrix}, \quad \begin{bmatrix} \alpha_1 \\ \alpha_2 \\ \alpha_3 \end{bmatrix} = \begin{bmatrix} 60^\circ \\ 180^\circ \\ 300^\circ \end{bmatrix}, \quad \begin{bmatrix} \beta_1 \\ \beta_2 \\ \beta_3 \end{bmatrix} = \begin{bmatrix} 60^\circ \\ 180^\circ \\ 300^\circ \end{bmatrix} $$

The position vector of E_i with respect to the fixed frame can be expressed as:

$$ {P_{ei}}^b = Q\cdot {P_{ei}}^e + P_e^b = \begin{bmatrix} r\cos\theta_2\sin\theta_3\sin\beta_i + r\sin\theta_2\cos\beta_i \\ r\cos\theta_3\sin\beta_i \\ r\sin\beta_i\sin\theta_2\sin\theta_3 - r\cos\beta_i\cos\theta_2 + z_e \end{bmatrix} = \begin{bmatrix} x_{ei}^b \\ y_{ei}^b \\ z_{ei}^b \end{bmatrix} \tag{1} $$

where Q is the rotation matrix of the moving frame with respect to the fixed frame. Equation (1) can be differentiated as follows:

$$ \begin{bmatrix} \delta x_{ei}^b \\ \delta y_{ei}^b \\ \delta z_{ei}^b \end{bmatrix} = \begin{bmatrix} -r\sin\theta_2\sin\theta_3\sin\beta_i + r\cos\theta_2\cos\beta_i & r\cos\theta_2\cos\theta_3\sin\beta_i & 0 & 0 & 0 & 0 \\ 0 & -r\sin\theta_3\sin\beta_i & 0 & 0 & 0 & 0 \\ r\sin\beta_i\cos\theta_2\sin\theta_3 + r\cos\beta_i\sin\theta_2 & r\sin\beta_i\sin\theta_2\cos\theta_3 & 0 & 0 & 0 & 1 \end{bmatrix} \begin{bmatrix} \delta\theta_2 \\ \delta\theta_3 \\ \delta\theta_z \\ \delta x_e \\ \delta z_y \\ \delta z_e \end{bmatrix} $$

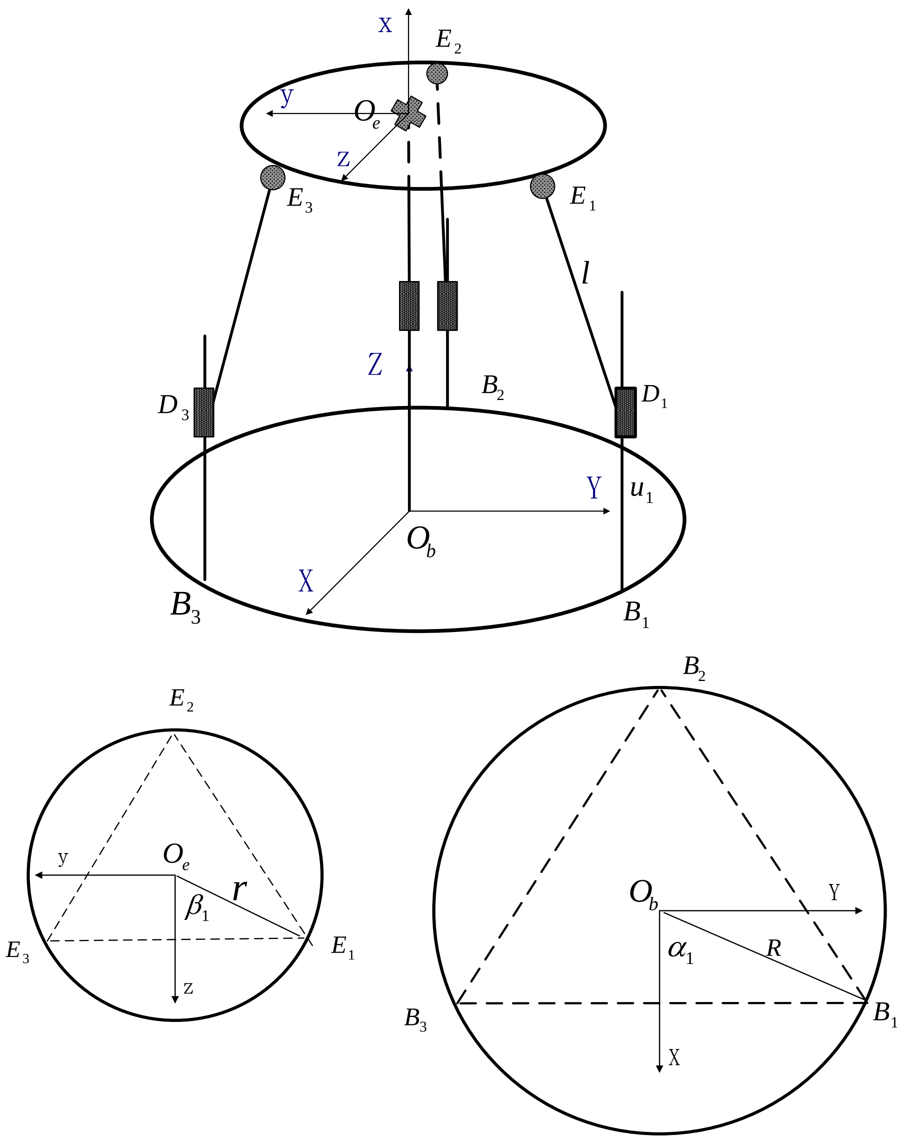

Figure 1. Schematic representation of the new 3PUS-PU mechanism.

Since the active legs have a fixed length, it can be shown that

$$\left|O_bE_i - O_bB_i - B_iD_i\right| = \left|D_iE_i\right| \qquad \text{(i=1,2,3)} \tag{2}$$

The above equation yields:

$$k_{i1}^{\ 2} + k_{i2}^{\ 2} + k_{i3}^{\ 2} = l_i^2 \tag{3}$$

where $k_{i1} = x_{ei}^b - R\cos\alpha_i$, $k_{i2} = y_{ei}^b - R\sin\alpha_i$, $k_{i3} = z_{ei}^{\ b} - u_i$
$u_i (i = 1,2,3)$ is the joint motion, which can be expressed as follows:

$$u_i = P_{ei}^{\ b}(3,1) - (l_i^2 - (P_{bi}^{\ b}(1,1) - P_{ei}^{\ b}(1,1))^2 - (P_{bi}^{\ b}(2,1) - P_{ei}^{\ b}(2,1))^2)^{1/2} \tag{4}$$

Equation (3) can be differentiated as:

$$\begin{bmatrix} \delta u_i \\ \delta l_i \end{bmatrix} = \begin{bmatrix} -\dfrac{k_{i1}}{k_{i4}} & -\dfrac{k_{i2}}{k_{i4}} & -\dfrac{k_{i3}}{k_{i4}} \\ \dfrac{k_{i1}}{l_i} & \dfrac{k_{i2}}{l_i} & \dfrac{k_{i3}}{l_i} \end{bmatrix} \cdot \begin{bmatrix} \delta x_{ei}^b \\ \delta y_{ei}^b \\ \delta z_{ei}^b \end{bmatrix} \tag{5}$$

where $k_{i4} = -k_{i3}$

The twist in the moving platform is expressed as $t = \begin{bmatrix} \delta\theta_2 & \delta\theta_3 & \delta\theta_z & \delta x_e & \delta y_e & \delta z_e \end{bmatrix}^T$

and

$$\dot{\rho} = \begin{bmatrix} \delta l_1 \\ \delta l_2 \\ \delta l_3 \end{bmatrix} = J_p \cdot t = \begin{bmatrix} \begin{bmatrix} \dfrac{k_{11}}{l_1} & \dfrac{k_{12}}{l_1} & \dfrac{k_{13}}{l_1} \end{bmatrix} \cdot J_1 \\ \begin{bmatrix} \dfrac{k_{21}}{l_2} & \dfrac{k_{22}}{l_2} & \dfrac{k_{23}}{l_2} \end{bmatrix} \cdot J_2 \\ \begin{bmatrix} \dfrac{k_{31}}{l_3} & \dfrac{k_{32}}{l_3} & \dfrac{k_{33}}{l_3} \end{bmatrix} \cdot J_3 \end{bmatrix} \cdot \begin{bmatrix} \delta\theta_2 \\ \delta\theta_3 \\ \delta\theta_z \\ \delta x_e \\ \delta y_e \\ \delta z_e \end{bmatrix} \tag{6}$$

KINETOSTATIC MODEL

The kinematic chain of the passive leg can be considered as a serial manipulator. The kinematic structure of the passive leg is illustrated in Figure 2. From Figure 2 one can obtain the D-H parameters of the passive leg, as shown in Table 1.

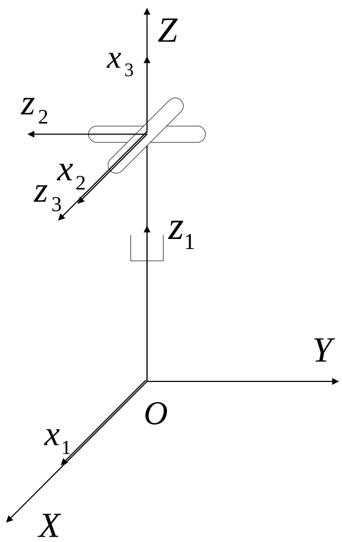

Figure 2. Kinematic structure of the passive le

Table 1. D-H parameters for the central passive leg.

i	a_i	d_i	α_i	θ_i
0	0	0	0	0
1	0	z_e	90°	0
2	0	0	90°	θ_2
3	0	0	0	θ_3

The Cartesian coordinate frame is used as frame 0, so that $\alpha_0 = 0^\circ, \theta_0 = 0^\circ$, then one obtains:

$$Q_{40} = \begin{bmatrix} 1 & 0 & 0 \\ 0 & 1 & 0 \\ 0 & 0 & 1 \end{bmatrix} \tag{7}$$

where Q_0 is the rotation matrix from the fixed reference frame to the first frame of the passive leg, and

$$Q_{41} = \begin{bmatrix} 1 & 0 & 0 \\ 0 & 0 & -1 \\ 0 & 1 & 0 \end{bmatrix}, \quad Q_{42} = \begin{bmatrix} \cos\theta_2 & 0 & \sin\theta_2 \\ \sin\theta_2 & 0 & -\cos\theta_2 \\ 0 & 1 & 0 \end{bmatrix}, \quad Q_{43} = \begin{bmatrix} \cos\theta_3 & -\sin\theta_3 & 0 \\ \sin\theta_3 & \cos\theta_3 & 0 \\ 0 & 0 & 1 \end{bmatrix}$$

The rotation matrix can be written as: $Q = Q_{40}Q_{41}Q_{42}Q_{43}$

Q_{41} is the rotation matrix from the first frame to the second frame of the passive leg; Q_{42} is the rotation matrix from the second frame to the third frame of the passive leg; and Q_{43} is the rotation matrix from the third frame to the final frame of the passive leg;

By multiplying equation (7) in each equation by e_{4i} and r_{4i}, one obtains the following:
$e_{41} = Q_{40}e_{40}$; $e_{42} = Q_{40}Q_{41}e_{40}$; $e_{43} = Q_{40}Q_{41}Q_{42}e_{40}$
where $e_{40} = \begin{bmatrix} 0 & 0 & 1 \end{bmatrix}^T$

The position vectors are expressed as:

$$\begin{gathered} r_{41} = Q_{40}a_{41} + Q_{40}Q_{41}a_{42} + Q_{40}Q_{41}Q_{42}a_{43} \\ r_{42} = Q_{40}Q_{41}a_{42} + Q_{40}Q_{41}Q_{42}a_{43}; \;\; r_{43} = Q_{40}Q_{41}Q_{42}a_{43} \end{gathered} \tag{8}$$

where $a_{4i} = \begin{bmatrix} a_i\cos\theta_i & a_i\sin\theta_i & d_i \end{bmatrix}$

For the central passive leg, one has the following equation:

$$J_4 \dot{\theta}_4 = t \tag{9}$$

where $\dot{\theta}_4 = \begin{bmatrix} \dot{\rho} & \dot{\theta}_2 & \dot{\theta}_3 \end{bmatrix}^T$

The Jacobian matrix of the central passive leg can be expressed as follows:

$$J_4 = \begin{bmatrix} 0 & e_{42} & e_{43} \\ e_{41} & e_{42} \times r_{42} & e_{43} \times r_{43} \end{bmatrix} \tag{10}$$

According to the principle of virtual work, the Cartesian compliance matrix of the 3PUS-PU mechanism can be derived as follows (Zhang, 2000):

$$C_c = J_4 (J_p J_4)^{-1} C (J_p J_4)^{-T} J_4^T \tag{11}$$

where $C = diag[c_1, c_2, c_3]$, c_i is the compliance of the i^{th} actuator, here we set c_i =0.001.

EFFECTS OF POSITION AND ORIENTATION PARAMETERS ON COMPLIANCE

We fixed $\theta_2 = 90^\circ$, and used the design kinematic parameters which are as follows:

R =0.4m; r =0.25m; l =0.5m; $\theta_3 \in [-50^\circ, 50^\circ]$, $z_e \in [0.3, 0.7]m$

Then, compliance mapping is obtained in each direction as shown in Figure 3. From Figure 3 one can see that when θ_3 =0, i.e. the moving platform is parallel to the base, a minimum compliance exists in the θ_x direction, which means a maximum stiffness exists in the θ_x direction. The value of z_e, which is the height of the moving platform, does not impose a fundamental influence on the compliance in the θ_x direction. As θ_3 increases, the compliance in the θ_x direction increases.

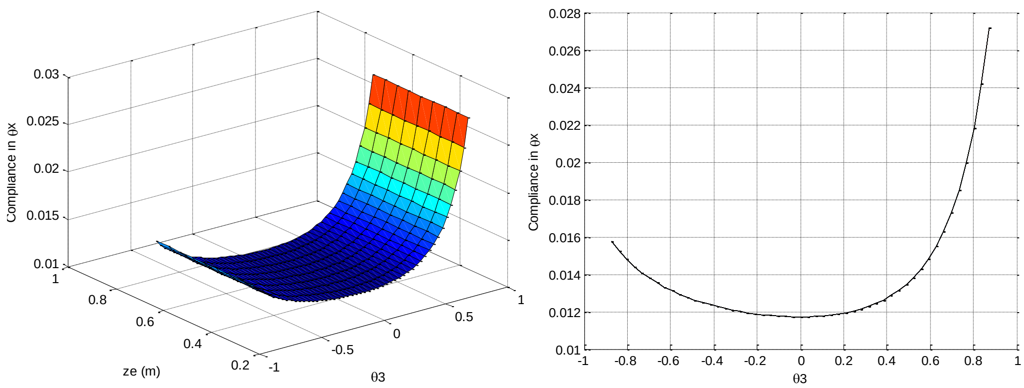

Figure 3. Compliance in the θ_x direction along with θ_3 and z_e.

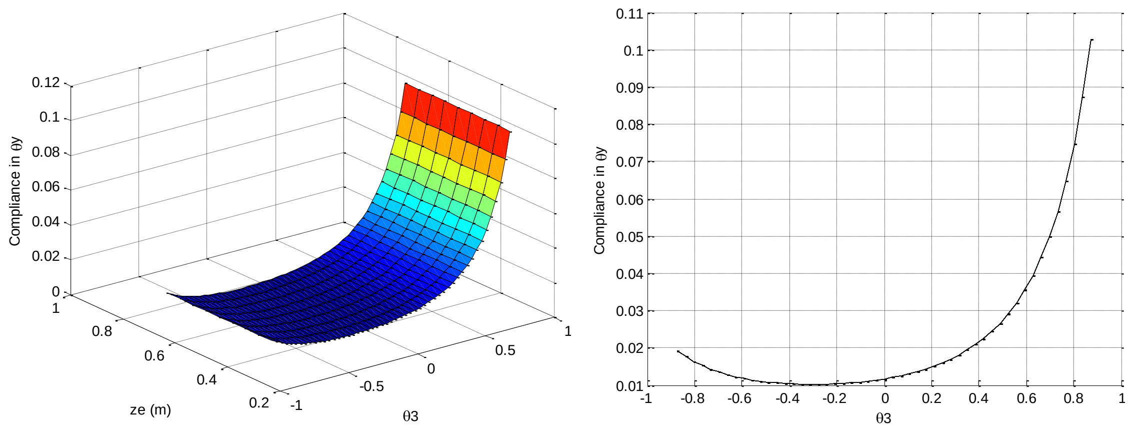

Figure 4. Compliance in the θ_y direction along with θ_3 and z_e

From Figure 4 one can see that when $\theta_3 = -17^{\circ}$, a minimum compliance exists in the θ_y direction, which means a maximum stiffness exists in the θ_y direction. The value of z_e, which is the height of the moving platform, does not impose a fundamental influence on the compliance in the θ_y direction. As θ_3 increases, the compliance in the θ_y direction increases.

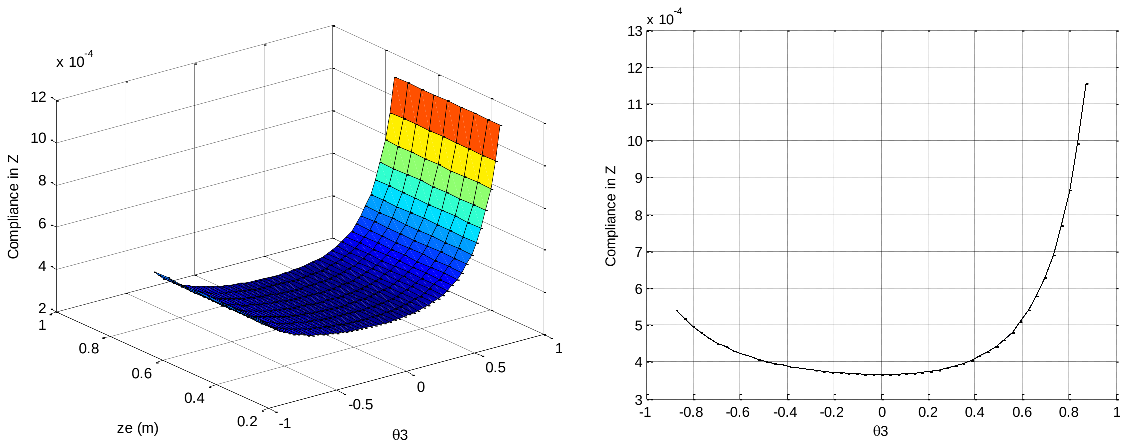

Figure 5. Compliance in Z direction along with θ_3 and z_e

From Figure 5 one can see that when $\theta_3 = 0^{\circ}$, i.e. the moving platform is parallel to the base, a minimum compliance exists in the Z direction, which means a maximum stiffness exists in the Z direction. The value of z_e does not impose a fundamental influence on the compliance in the Z direction. As θ_3 increases, the compliance in the Z direction increases.

EFFECTS OF GEOMETRIC PARAMETERS ON COMPLIANCE

The effects of R and r on compliance

In addition we fixed $\theta_2 = 90^\circ$, and use the following design kinematic parameters: l=0.5m; $\theta_3 = 0^\circ$, $z_e = 0.5m$, $R \in [0.3, 0.6]m$, $r \in [0.15, 0.25]m$

The compliance mapping along with the change in R and r can be obtained in Figure 5. It can be seen that when R=0.3 m, r=0.25 m, a minimum compliance exists in the θ_x direction, which means a maximum stiffness exists in that direction. From Figure 7 one can see that the effects of R and r on the compliance in the θ_y direction is the same as in the θ_x direction. From Figure 8 one can see that when R=0.3 m, r=0.25 m, the compliance in the Z direction achieves the minimum value.

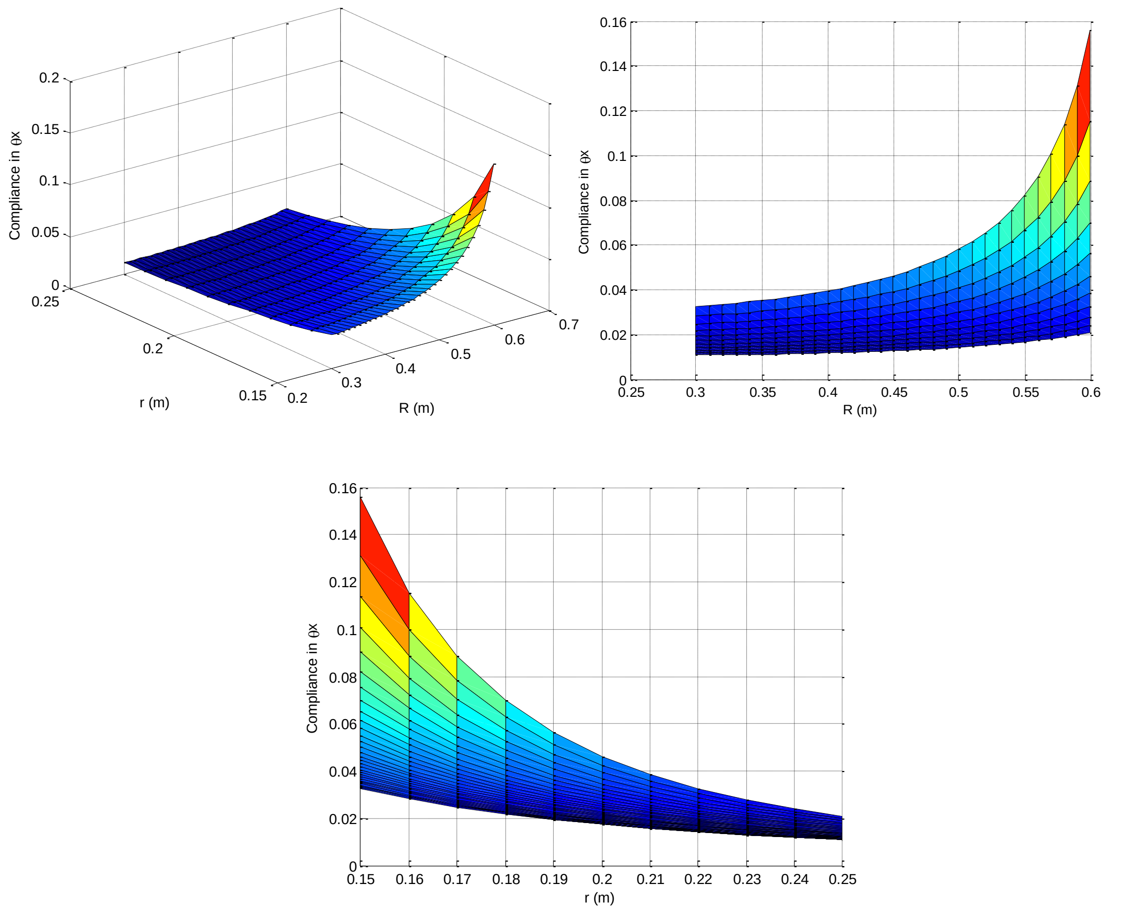

Figure 6. Compliance in the θ_x direction along with R and r.

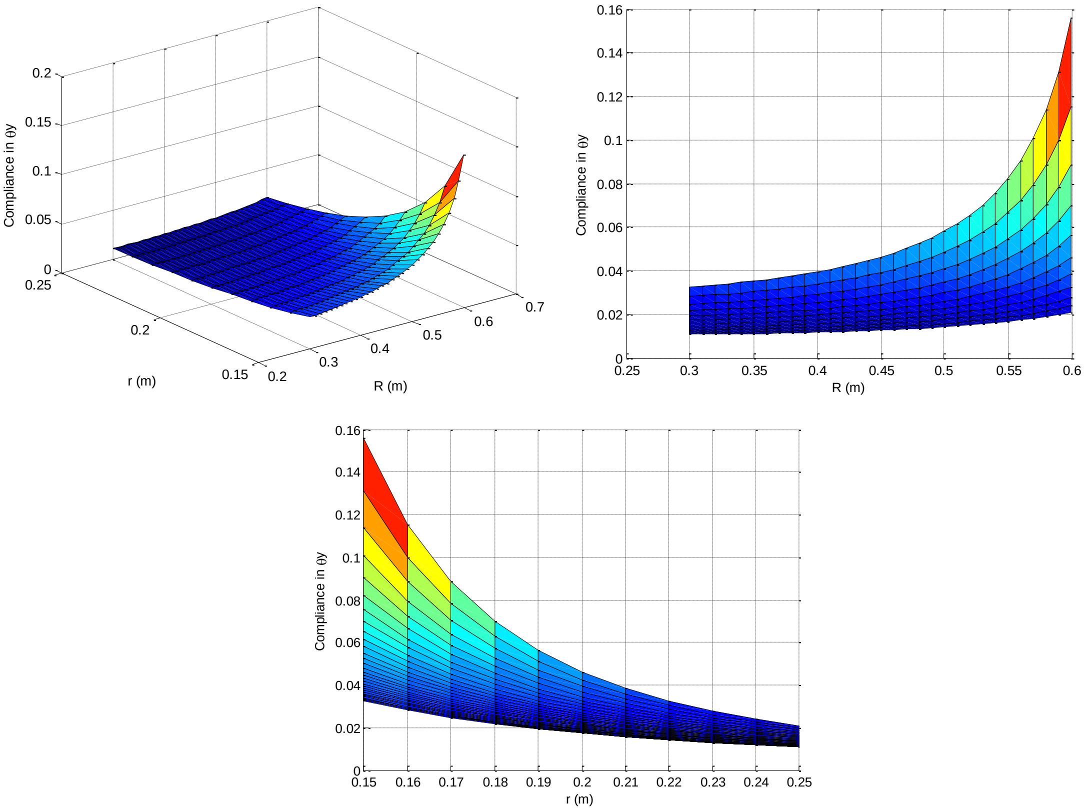

Figure 7. Compliance in the θ_y direction along with R and r.

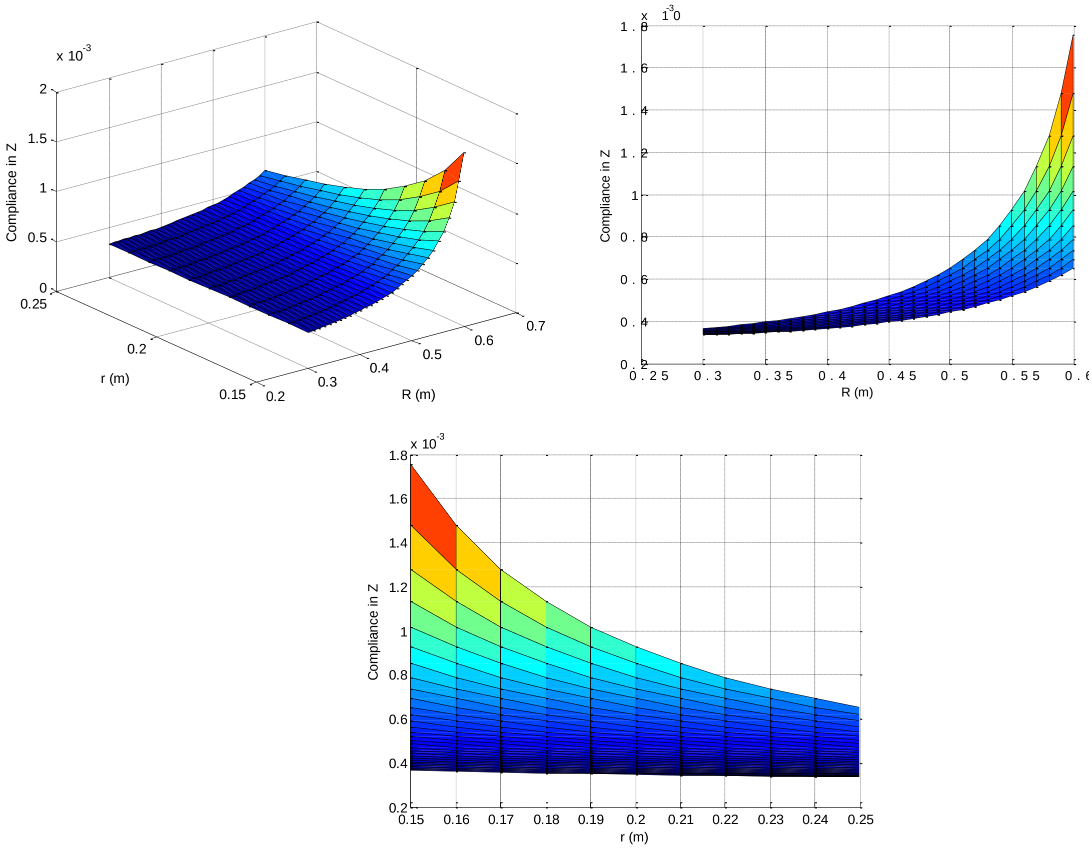

Figure 8. Compliance in the Z direction along with R and r.

The effects of l on compliance

We fixed $\theta_2 = 90^\circ$, and used the design kinematic parameters which are as follows: $\theta_3 = 0^\circ$, $z_e = 0.5m$, $r = 0.25m$, $R = 0.4m$, $l \in [0.45, 0.65]m$, then we can obtain the trends in the compliance in each direction, along with the change in the length of the active legs as follows.

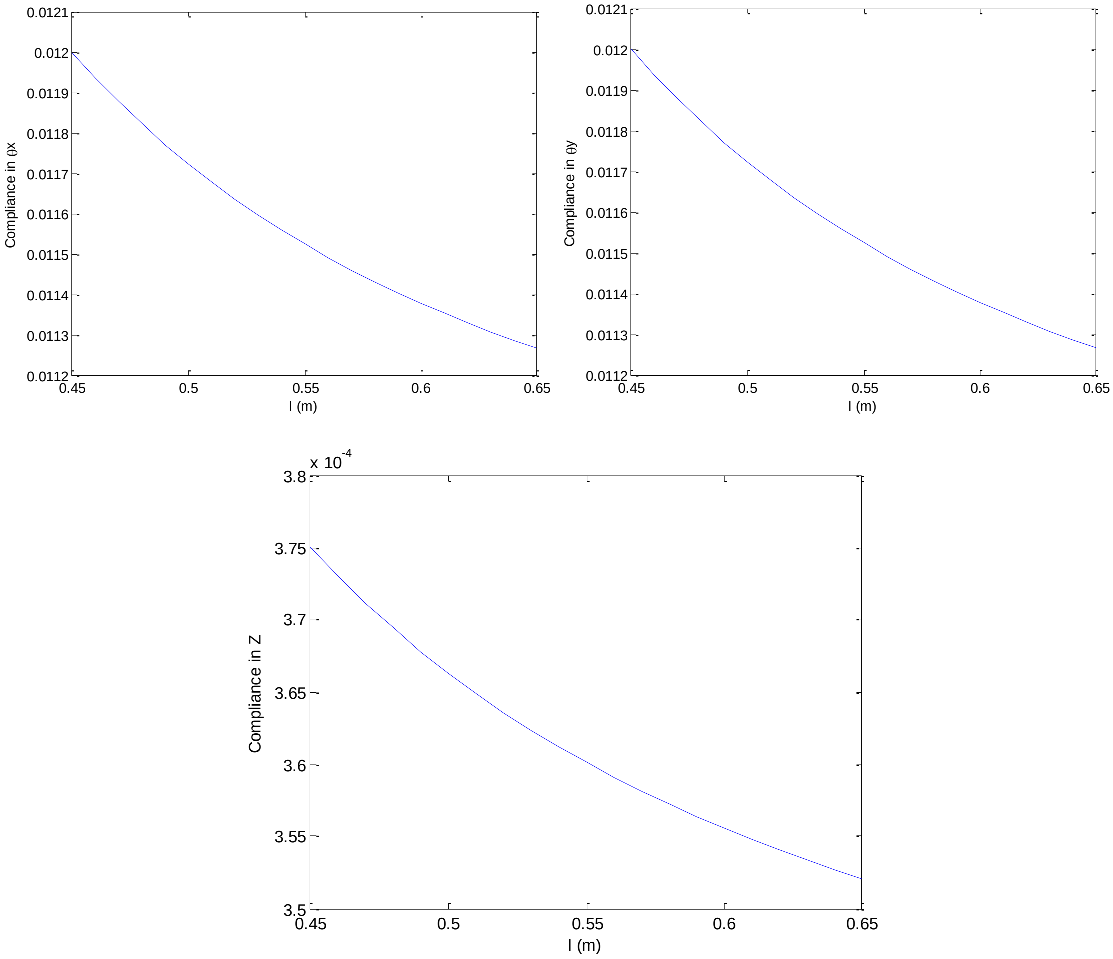

Figure 9. Compliance in the θ_x, θ_y, Z directions along with l.

From Figure 9 one can see that the compliance in the θ_x, θ_y and Z directions reduces as l becomes longer. When setting $\theta_3 = -17^\circ$, $z_e = 0.5m$, $r = 0.25m$, $R = 0.4m$, $l \in [0.45, 0.65]m$ one has the following trends. From Figure 10 one can see that the compliance in the θ_x and Z directions reduces as l becomes longer, and the compliance in the θ_y direction increases as l becomes longer. After many experiments, we conclude that these geometric parameters and the position and orientation parameters all affect the compliance of the mechanism in each direction. The leading diagonal element of the compliance matrix is the manipulator's pure compliance in each direction. The sum of the leading diagonal elements of the compliance matrix is defined as the global compliance. The global compliance is related to system rigidity, and we want the global compliance to be as small as possible. Next, we need to determine these geometric parameters and the position and orientation parameters simultaneously to obtain the minimum summation of the leading diagonal elements of the compliance matrix of the mechanism.

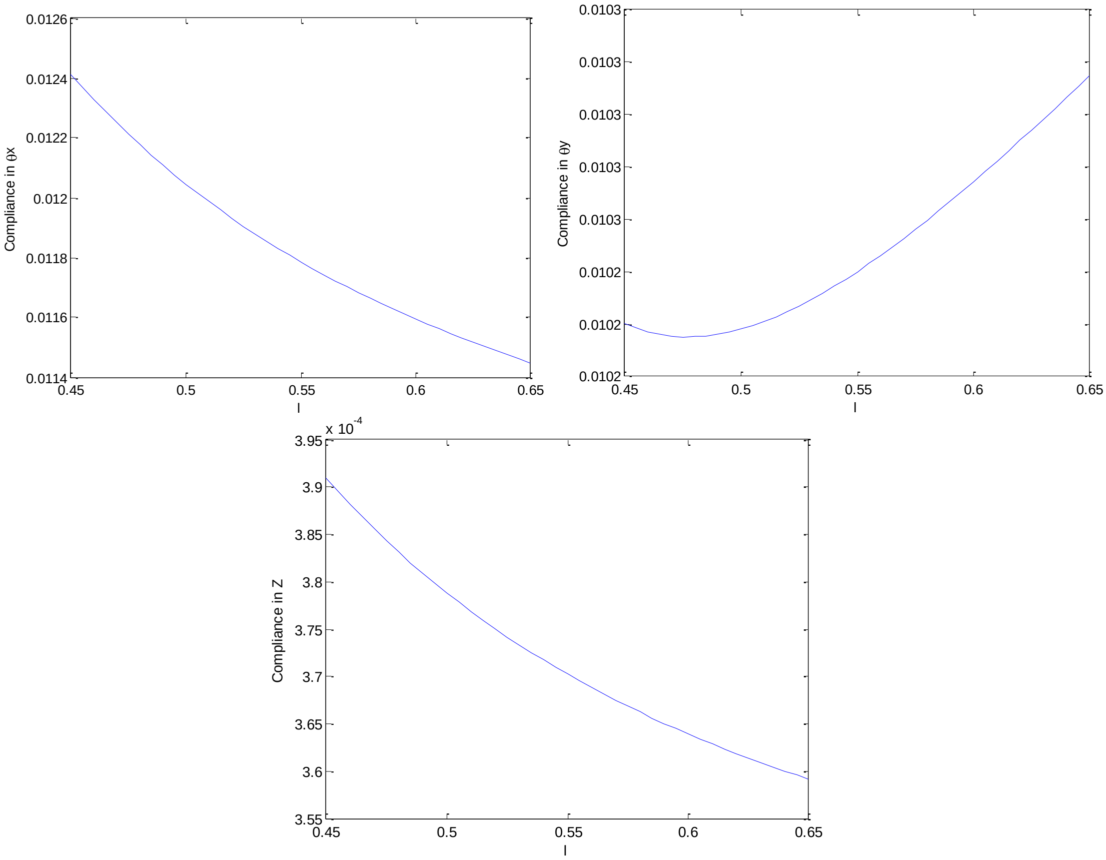

Figure 10. Compliance in the θ_x, θ_y, Z directions along with l

OPTIMISATION

Traditional optimisation methods use a local search by a convergent stepwise procedure, which compares the values of the following points and then moves to the optimal points. Global optima can only be found if the problem has certain convexity properties which guarantee any local optima is a global optimum It faces the danger of falling in local optima. However, genetic algorithms are based on the population-to-population rule; which can escape from local optima Genetic algorithms have the advantages of good convergence and robustness properties: such as the following,

(i) They require no knowledge or gradient information about the optimisation problems; they can solve any kind of objective functions and any kind of constraints defined on discrete, continuous or mixed search spaces;
(ii) Discontinuities present on optimisation problems have little effect on the overall optimisation performance;
(iii) It is effective at performing global search instead of local optima;
(iv) It performs very well on large-scale optimisation problems;
(v) They can be employed on a wide variety of optimisation problems.

Since global compliance is related to system rigidity, and the geometric parameters and position and orientation parameters all affect the compliance of the mechanism in each direction as stated in sections 4 and 5, we will use the genetic algorithm (GA) to optimise the global compliance by adjusting the geometric parameters and position and orientation parameters simultaneously. The objective function for optimisation is as follows:

$$y = C_c(1,1) + C_c(2,2) + C_c(3,3) + C_c(4,4) + C_c(5,5) + C_c(6,6) \tag{12}$$

Design variables are R, r, l, θ_2, θ_3 and z_e

Constraints are set as follows:

$R \in [0.3, 0.6]m$, $r \in [0.15, 0.25]m$, $l \in [0.45, 0.65]m$, $\theta_2 \in [40^\circ, 140^\circ]$, $\theta_3 \in [-50^\circ, 50^\circ]$, $z_e \in [0.3, 0.7]m$

Run the GA solver, and the following result is obtained:

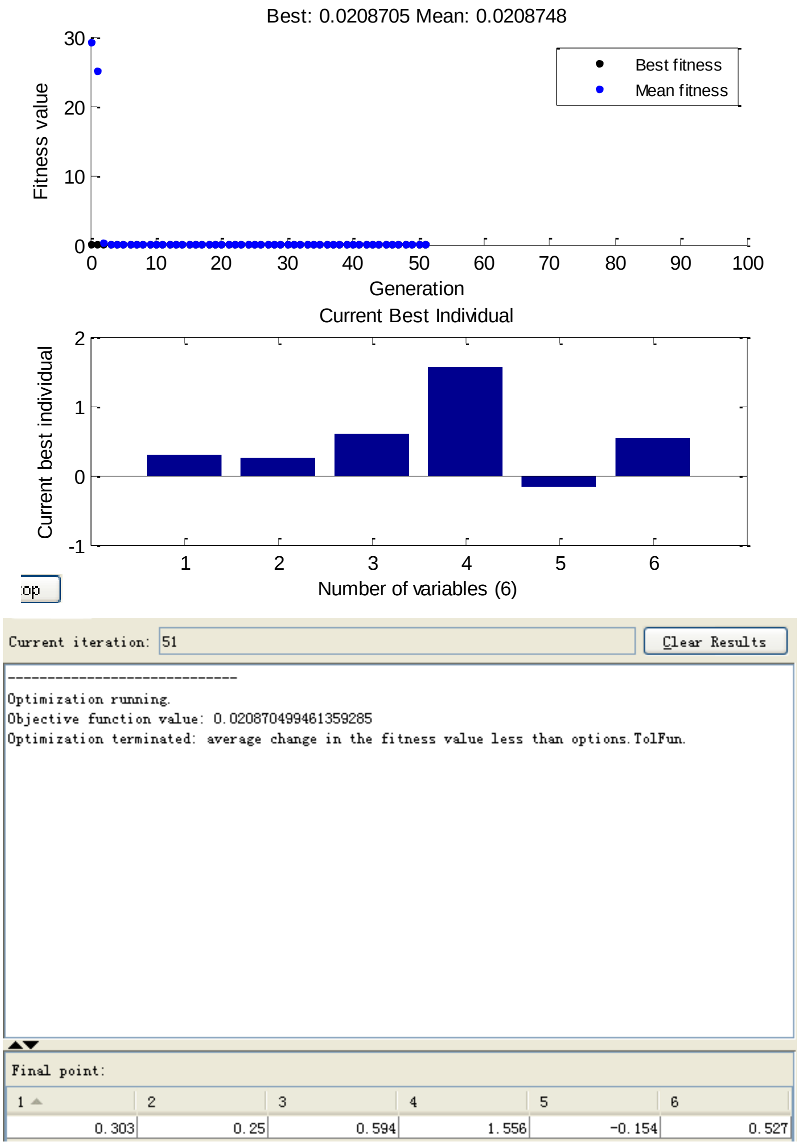

Figure 11. Optimisation results.

After optimisation, when $R = 0.303m$, $r = 0.25m$, $l = 0.594m$, $\theta_2 = 89^\circ$, $\theta_3 = -8.7^\circ$, $z_e = 0.527m$, the compliance sum which is the global compliance reaches the minimum value of 0.02087.

COMPLIANCE COMPARISON BETWEEN TWO 3PUS-PU MECHANISMS

The guide-ways of the new 3PUS-PU mechanism are parallel to each other. However, if the guide-ways are not parallel to each other, but rather intersecting each other as shown in Figure 12(b), here we compare these two mechanisms' compliance in each direction. The angle between the guide-ways and the base is φ.

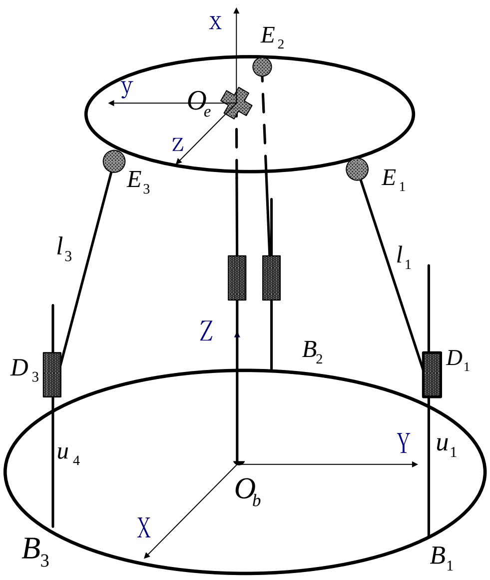

(a) Parallel guide-ways

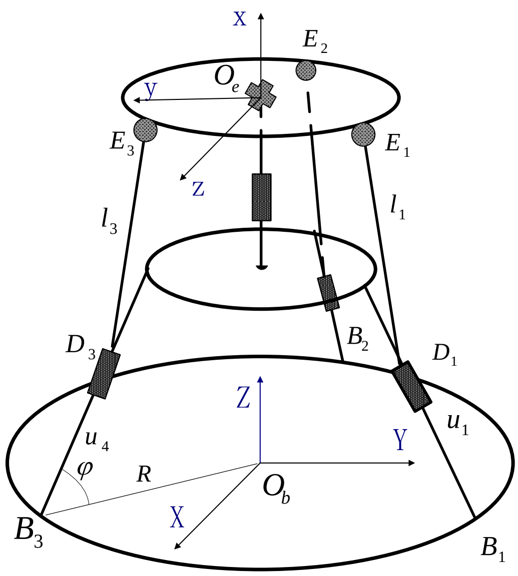

(b) Intersecting guide-ways

Figure 12. Two kinds of 3PUS-PU mechanism

When $\varphi = 50^\circ$, $R = 0.05m$, $r = 0.025m$, $l = 0.12m$, $\theta_2 = 90^\circ$, $\theta_3 \in [-50^\circ, 50^\circ]$, $z_e \in [0.03, 0.06]m$, the compliances in each direction for the two mechanisms are shown in Figure 13, the upper plot figure presents the compliance for the mechanism with intersecting guide-ways, and the lower figure presents the compliance for the new mechanism with parallel guide-ways. One can clearly see that when the structural parameters are very small, the compliance of the mechanism with intersecting guide-ways is larger than that of the new mechanism with parallel guide-ways, which means that the stiffness of the new mechanism is better than that of one with intersecting guide-ways.

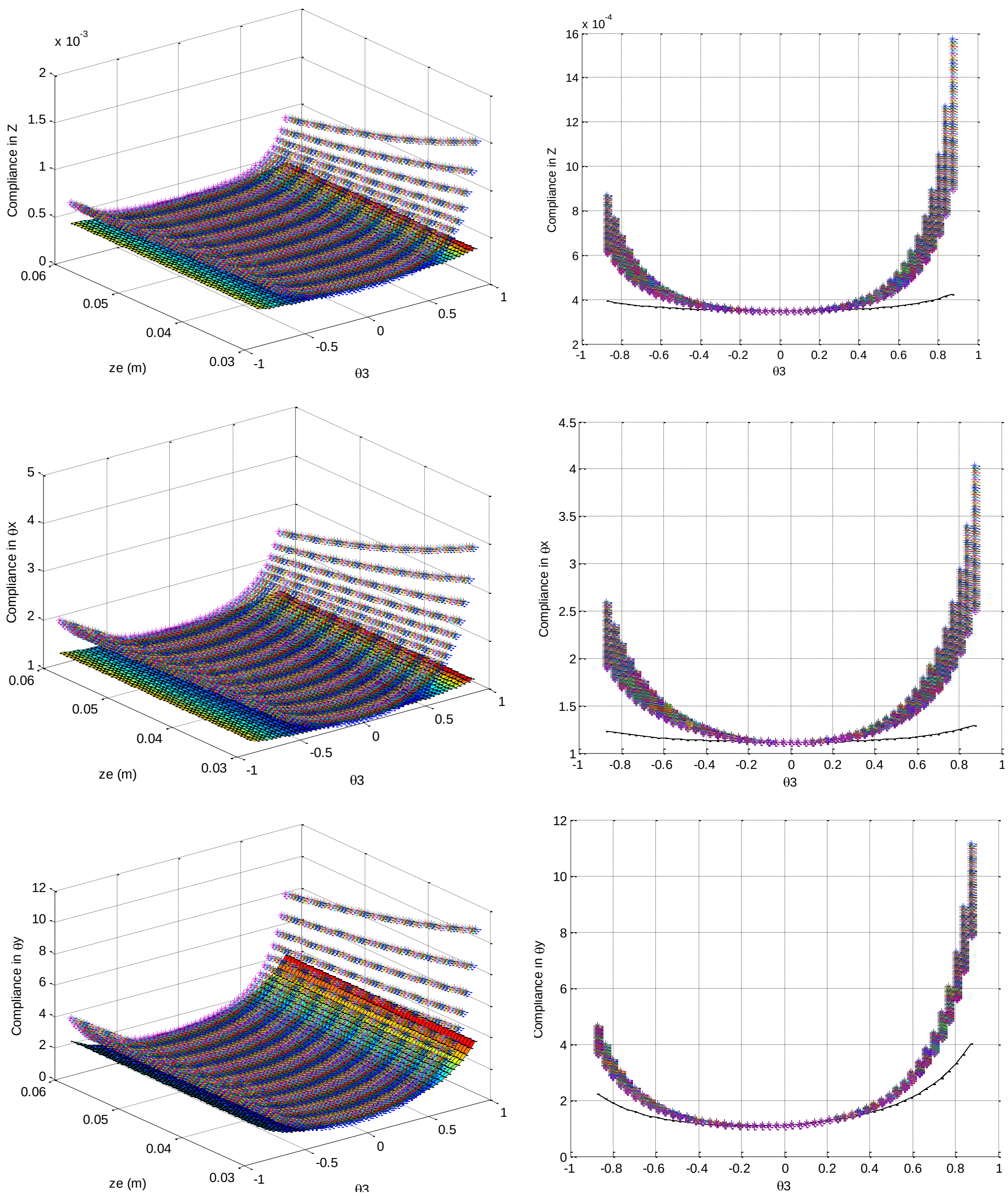

Figure 13. Compliance comparison between two mechanisms when the structural parameters are small.

When $\varphi = 50^\circ$, $R = 0.37m$, $r = 0.075m$, $l = 0.353m$, $\theta_2 = 90^\circ$, $\theta_3 \in [-50^\circ, 50^\circ]$, $z_e \in [0.45, 0.6]m$, the compliance in each direction of those two mechanisms are presented in Figure 14. One can also see that the compliance in each direction for the mechanism with intersecting guide-ways is smaller than those of the new mechanism with parallel guide-ways, which means the stiffness for the system with intersecting guide-ways is better than that of the new mechanism with parallel guide-ways when the structural parameters are large.

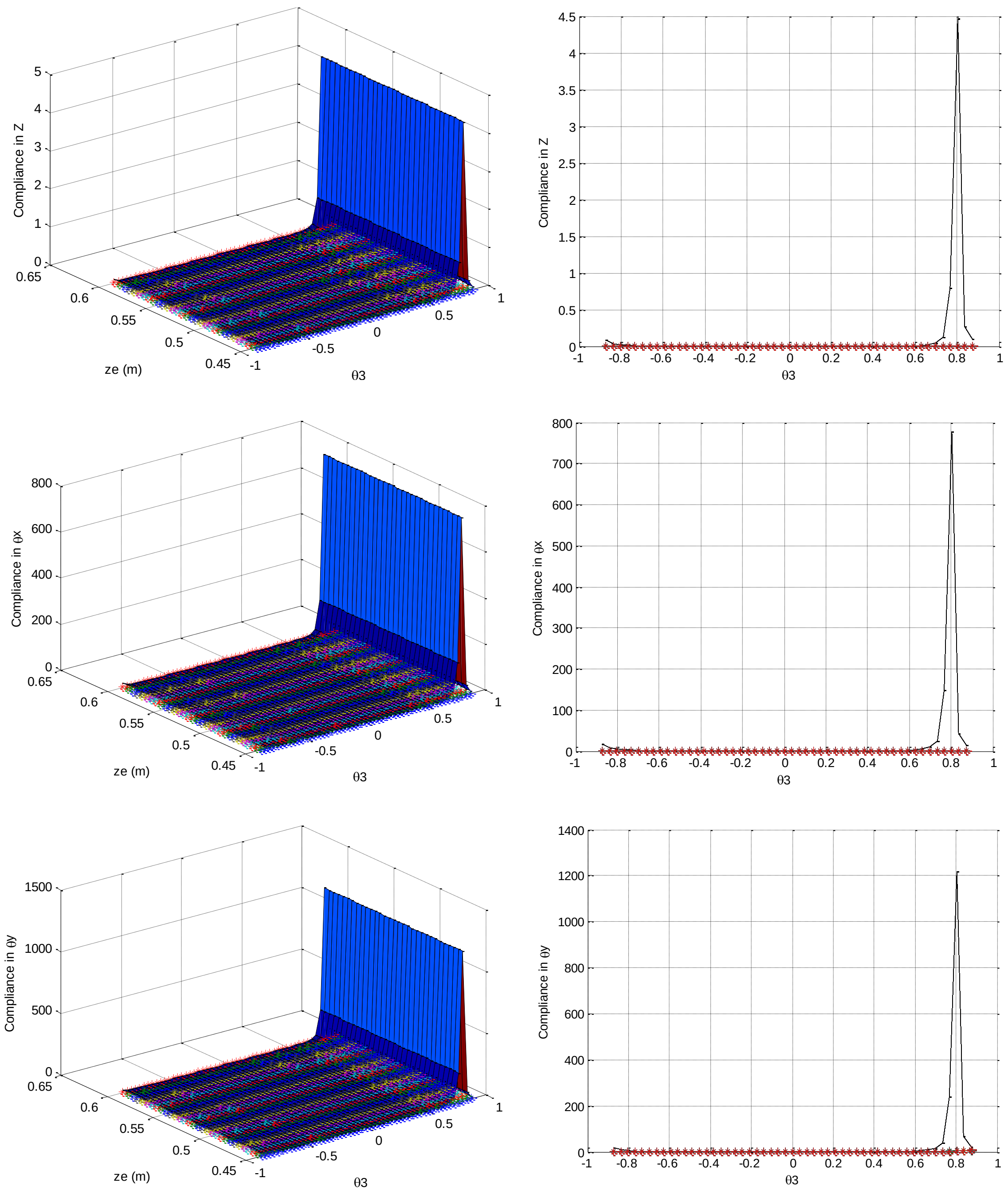

Figure 14. Compliance comparison between two mechanisms when the structural parameters are large.

CONCLUSION

The article investigates the compliance of a new 3PUS-PU mechanism, and compares the compliance of two similar 3PUS-PU mechanisms. The effects the geometric parameters and position and orientation parameters on the compliance of the new 3PUS-PU mechanism in each direction is analysed, and the genetic algorithm is used to optimise the global compliance by adjusting the design variables. It is found that the global compliance reaches the minimum value when R=0.303 m, r = 0.25 m, l = 0.594 m, $\theta_2 = 89^o$, $\theta_2 = -8.7^o$, z_e = 0.527 m. Secondly, the compliance of two similar kinds of 3PUS-PU mechanism in each direction are compared, and it is shown that the stiffness of the mechanism with intersecting guide-ways in each direction is smaller than that of the new mechanism with parallel guide-ways when the structural parameters are very small. However the stiffness of the mechanism with intersecting guide-ways in each direction is larger than that of the new mechanism with parallel guide-ways when the structural parameters are relatively large, which provides engineers with a guide to selecting the correct mechanism type according to their different practical requirements and scenarios, such as whether it is to be used in machine tools or micromanipulation. For future work, a prototype should be fabricated based on the proposed model to test the theoretical results.

REFERENCES

Hu, Y., Li, B., Hu, H. and Ying, W. 2006. Kinematics, workspace and dexterity analysis for a 4PUS-1RPU parallel kinematic platform. Proceedings of the 7th International Conference on Frontiers of Design and Manufacturing Sciences (ICFDM), pp. 455-458.

Li, Y.M. and Xu, Q.S. 2008. Design, analysis and applications of a class of new 3-DOF translational parallel manipulators. In: Ryu, J.-H. (ed.) Parallel Manipulators, New Development, pp. 457-482.

Pan, M. 2011. Improved design of a three-degree of freedom hip exoskeleton based on biomimetic parallel structure. Master thesis, University of Ontario Institute of Technology, Canada.

Patel, Y.D. and George, P.M. 2012. Parallel manipulators applications - a survey. Modern Mechanical Engineering, 2: 57-64.

Tsai, L.W. and Joshi, S. 2002. Kinematic analysis of 3-DOF position mechanisms for use in hybrid kinematic machines. Journal of Mechanical Design, 124: 245-253.

Wu, C., Liu, X.J., Wang, L.P. and Wang, J.S. 2011. Dimension optimization of an orientation fine-tuning manipulator for segment assembly robots in shield tunneling machines. Automation in Construction, 20(4): 353-359.

Xi, F.F., Zhang, D., Mechefske, C.M. and Lang, S.Y.T. 2004. Global kinetostatic modeling of tripod-based parallel kinematic machine. Mechanism and Machine Theory, 39: 357-377.

Yu, H.J. 2010. Research on parallel robot based flexible fixtures for automotive sheet metal assembly. PhD thesis, Harbin Institute of Technology, China.

Zhang, D. 2000. Kinetostatic analysis and optimization of parallel and hybrid architecture for machine tools. PhD thesis, Laval University, Canada.

Zhang, D. 2009. Parallel robotic machine tools. Springer.

Zhang, D., Gao, Z., Song, B. and Ge, Y.J. 2009. Configuration design and performance analysis of a multidimensional acceleration sensor based on 3RRPRR decoupling parallel mechanism. Joint 48th IEEE Conference on Decision and Control and 28th Chinese Control Conference, pp. 8304-8309.

Zhang, D., Wang, L.H. and Lang, S.Y.T. 2005. Parallel kinematic machines: design, analysis and simulation in an integrated virtual environment. Journal of Mechanical Design, 127: 580-588.